

Cite this: *J. Mater. Chem. C*, 2020, **8**, 7882

# A probe of the radiation field magnetic component based on octahedral Yb<sup>3+</sup> in the CaNbGa garnet – CNGG – single crystal†

Jorge Omar Álvarez-Pérez,<sup>id</sup> José María Cano-Torres,<sup>id</sup>  
María Dolores Serrano,<sup>id</sup> Concepción Cascales<sup>id</sup> and Carlos Zaldo<sup>id</sup>\*

In a disordered Yb<sup>3+</sup>-doped CaNbGa garnet – CNGG – single crystal, it is shown that octahedral Yb centers exist up to a solubility limit of about  $5 \times 10^{18} \text{ cm}^{-3}$  in addition to the well known dodecahedral Yb which incorporates to a much larger density  $\sim 10^{21} \text{ cm}^{-3}$ . Despite the low density of the octahedral Yb, the presence of a symmetry center for this garnet site forbids electric dipole (ED) transitions, thus magnetic dipole (MD) spectroscopic contributions are observed with an intensity similar to that of ED ones. Because of the easy growth of this garnet, the potential application of these two contributions for probing the magnetic field component radiated by plasmonic structures is discussed on the basis of time-resolved spectroscopy, since ED Yb<sup>3+</sup> photoluminescence is about one order of magnitude faster than MD  ${}^2F_{5/2} \rightarrow {}^2F_{7/2}$  ( $\Delta J = +1$ ) emissions for the 0.3 at%Yb:CNGG crystal. Channels appropriated for room temperature operation can be excited at  $\lambda_{\text{EXC}} = 960.3 \text{ nm}$ , while sensed at  $\lambda_{\text{EMI}} = 1022 \text{ nm}$  for the short-lived ED reference channel and  $\lambda_{\text{EMI}} = 998, 1011, 1068$  or  $1080 \text{ nm}$  for the long-lived MD signal channel.

Received 30th March 2020,  
Accepted 30th April 2020

DOI: 10.1039/d0tc01608j

rsc.li/materials-c

## 1. Introduction

Energy levels of trivalent lanthanides (Ln<sup>3+</sup>) are characterized by  ${}^{2S+1}L_J$  multiplets further split by the crystal field (CF) of a host in  $m_J$  levels. Intraconfigurational electronic transitions between these multiplets are most often induced by light-matter interactions mediated by electric fields through forced electric dipole (ED) transitions, but also include magnetic dipole (MD) interactions, particularly notable for transitions between multiplets with  $\Delta J = 0$  or  $\pm 1$ .<sup>1</sup> Although it is usually assumed that MD transitions are  $\sim 10^5$  times weaker than ED ones, their relative intensity in fact depends on the specific selection rules. In hosts where ED transitions are weak or even strictly forbidden, as when Ln<sup>3+</sup> are incorporated at sites with a center of symmetry, the intensity of MD transitions can be dominant.

Stimulated by recent advances in optical plasmonic-based metamaterials and nanophotonics, a variety of ways to exploit MD transitions of Ln<sup>3+</sup> have been proposed: theoretically, as the

building blocks for homogeneous negative index materials,<sup>2</sup> or experimentally, as probes for the study of local magnetic fields in metamaterials, in a very simple approach that consists of placing the MD probe at the metamaterial surface, and if this resonance frequency corresponds to the spectral range of the field enhancement, spectral changes in intensity or shape may be observed in comparison with other magnetic dipoles outside the system or with some reference ED emission in the same system.<sup>3–7</sup> Furthermore, experimental studies by using the competition between ED and MD processes have shown the way for achieving a strong enhancement of MD emission<sup>8</sup> and also to broadly tune the emission spectra.<sup>9</sup>

For the above indicated sensing purposes, previous studies have involved mainly the visible  ${}^5D_0 \rightarrow {}^7F_1$  MD transition of Eu<sup>3+</sup>, in probing systems based on Eu-doped Y<sub>2</sub>O<sub>3</sub> thin films,<sup>7–9</sup> dispersions of Eu-doped organic systems in polymeric thin films,<sup>3,4,6</sup> or Eu-doped Y<sub>2</sub>O<sub>3</sub> NPs (about 60 nm).<sup>10</sup> The specific advantage of using Eu<sup>3+</sup> is the coexistence of the nearly pure MD  ${}^5D_0 \rightarrow {}^7F_1$  ( $\lambda \approx 590 \text{ nm}$ ) transition and the ED  ${}^5D_0 \rightarrow {}^7F_2$  ( $\lambda \approx 615 \text{ nm}$ ) transition used as the reference. Other Ln<sup>3+</sup> emissions which have been tested with the same aim are mixed MD–ED transitions in the near-infrared (NIR) range, for instance the overlapping  ${}^4F_{9/2} \rightarrow {}^6F_{11/2} + {}^6H_{9/2}$  ( $\lambda \approx 734 \text{ nm}$ ) emissions of Dy<sup>3+</sup>,<sup>11</sup> the also overlapping  ${}^1G_4 \rightarrow {}^3H_5$  ( $\lambda \approx 784 \text{ nm}$ ) and  ${}^3H_4 \rightarrow {}^3H_6$  ( $\lambda \approx 800 \text{ nm}$ ) emissions of Tm<sup>3+</sup>,<sup>11</sup> or the  ${}^4I_{13/2} \rightarrow {}^4I_{15/2}$  ( $\lambda \approx 1.5 \mu\text{m}$ ) transition of Er<sup>3+</sup>,<sup>12</sup> in all cases by using the corresponding doped Y<sub>2</sub>O<sub>3</sub> thin films.

*Instituto de Ciencia de Materiales de Madrid, Consejo Superior de Investigaciones Científicas, c/Sor Juana Inés de la Cruz 3, 28049 Madrid, Spain.*  
E-mail: cezaldo@icmm.csic.es

† Electronic supplementary information (ESI) available: (i) Detailed comparative optical spectroscopy of dodecahedral and octahedral Yb<sup>3+</sup> centers in CNGG crystals. (ii) Detailed procedures of crystal field analyses applied to octahedral Yb<sup>3+</sup> centers in 0.3 at%Yb:CNGG crystals. (iii) Crystal field splitting of  ${}^2F_J$  Yb<sup>3+</sup> levels and the barycenter law. See DOI: 10.1039/d0tc01608j



The near-infrared (NIR) range from 800 to 1100 nm has several advantages over other spectral regions. As compared to the visible (characteristic of  $\text{Eu}^{3+}$ ), micron-sized plasmonic nanostructures are much easier to fabricate than nano-sized ones and their resonances exhibit higher-quality factors due to lower ohmic losses. However, as compared with the  $^4\text{I}_{13/2} \rightarrow ^4\text{I}_{15/2}$   $\text{Er}^{3+}$  transition at  $\lambda \approx 1.5 \mu\text{m}$ , emissions at  $\lambda < 1100 \text{ nm}$  can be observed using standard Si photodetector technology, which simplifies the detection process. Moreover, among MD  $\text{Ln}^{3+}$  emissions at this wavelength range, those that can be pumped at the NIR will be the better candidates to be used. From the above considerations the  $^2\text{F}_{5/2} \leftrightarrow ^2\text{F}_{7/2}$  transitions of  $\text{Yb}^{3+}$  (typically  $\lambda_{\text{EXC}} \approx 940\text{--}980 \text{ nm}$  and  $\lambda_{\text{EMI}} \approx 980\text{--}1060 \text{ nm}$ ) in a centrosymmetric crystal site are very interesting options. The simple two-state energy structure of  $\text{Yb}^{3+}$  means that MD emission can account for a significant contribution to the overall decay. In fact, relatively long  $\text{Yb}^{3+}$  lifetime ( $\tau$ ) characteristics of MD transitions have been measured for Yb-doped  $\text{BaF}_2$  and  $\text{SrF}_2$  fluorites ( $\tau = 9.72 \text{ ms}$  and  $8.20 \text{ ms}$ , respectively), as well as for  $\text{Rb}_2\text{NaYF}_6$  elpasolite ( $\tau = 10.84 \text{ ms}$ ) crystals, with  $\text{Yb}^{3+}$  at centrosymmetric sites of cubic eightfold and perfect octahedral coordination,<sup>13</sup> respectively, in both cases with calculated MD branching ratios of  $\sim 50\%$ .<sup>12</sup>

Cubic garnets  $\text{A}_3\text{M}_2\text{N}_3\text{O}_{12}$  with space group  $Ia\bar{3}d$  (No. 230) offer simultaneously non centrosymmetric dodecahedral 24c sites (A) and octahedral 16a centrosymmetric sites (M) to host Ln. An illustration of the garnet structure can be seen in the general view given in Fig. 1a. Fig. 1b shows the coordination of dodecahedral  $\text{AO}_8$  and octahedral  $\text{MO}_6$  garnet sites. Further drawings showing other atomic arrangements can be seen for instance in ref. 14. The  $\text{Ln}^{3+}$  distribution over 24c and 16a garnet sites is a topic which has been addressed with several purposes and under different approaches.<sup>15–23</sup> The main factor governing the site preference of  $\text{Ln}^{3+}$  in the garnet structure is the ionic size, in such a way that garnets with any  $\text{Ln}^{3+}$  cation occupying the dodecahedral 24c site are known,<sup>15</sup> and only the smallest size  $\text{Ln}^{3+}$  cations, typically  $\text{Dy}^{3+}$  to  $\text{Lu}^{3+}$  and also  $\text{Y}^{3+}$  or  $\text{Sc}^{3+}$ , are able to enter into the octahedral 16a site, even up to its complete filling, but in this case a 24c cation with a considerably large size, for example  $\text{Ca}^{2+}$  in the germanate series  $\text{Ca}_3\text{Ln}_2\text{Ge}_3\text{O}_{12}$ ,<sup>18</sup> including  $\text{Ca}_3\text{Y}_2\text{Ge}_3\text{O}_{12}$ ,<sup>20</sup> is required, thus the relative sizes of 24c and 16a cations also play a role. The presence of  $\text{Yb}^{3+}$  in

both garnet sites would offer the possibility of having the MD probe and ED reference ions in the same tested volume minimizing uncertainties related to excitation and detection processes, but so far the properties of Yb coexisting in both garnet sites have not been properly documented. Either the studies are limited to crystallographic aspects,<sup>16,17,20</sup> or the spectroscopic-based proposals<sup>21,23</sup> are not soundly supported by crystallographic data and/or crystal field (CF) interaction calculations.

In this work we present the first report and characterization of the  $^2\text{F}_{5/2}(n') \leftrightarrow ^2\text{F}_{7/2}(n)$  MD transitions of  $\text{Yb}^{3+}$  at the octahedral 16a (centrosymmetric  $C_{3i}$  symmetry) site of the  $\text{CaNbGa}$  garnet (thereafter CNGG). The host selection is based on the large  $\text{Ca}^{2+}$  ionic size filling the dodecahedral site, see before, while a large variety of ionic filling ( $\text{Nb}^{5+}$ ,  $\text{Ga}^{3+}$  and even vacancies) is found for the octahedral and tetrahedral sites of this garnet composition. The occupancy of the 24c dodecahedral site of the CNGG garnet by  $\text{Yb}^{3+}$  is well documented from both crystallographic and spectroscopic points of view.<sup>24–27</sup>

The emphasis of the present work is the study of  $\text{Yb}^{3+}$  in the octahedral 16a CNGG garnet site. Through low temperature (6 K) optical absorption (OA) and photoluminescence (PL) spectra followed by the modeling of CF interactions, it has been possible to establish the sequence of 16a  $\text{Yb}^{3+}$  energy levels as a well-separated set with regards to those of  $\text{Yb}^{3+}$  at the 24c dodecahedral site. The lifetime associated with the 16a  $\text{Yb}^{3+}$   $^2\text{F}_{5/2} \rightarrow ^2\text{F}_{7/2}$  MD emissions has been also measured, and the MD branching ratio has been calculated as  $\beta_{\text{MD}} = 50\%$ , a value that equals those of previously indicated for  $\text{Yb}^{3+}$  in centrosymmetric sites of fluoride-based hosts.<sup>12</sup> Furthermore, by using their different kinetics, ED and MD  $\text{Yb}^{3+}$  PL contributions have been separated even at room temperature (RT), opening the possibility of its application as a sensor for the magnetic field radiation in plasmonic systems.

## 2. Methods

### 2.1 Crystal growth

The crystal precursor polycrystalline material with a nominal cationic composition  $\text{Ca}_{2.991}\text{Yb}_{0.009}\text{Nb}_{1.6875}\text{Ga}_{3.1875}$  (0.3 at%Yb: CNGG) was prepared by mixing  $\text{CaCO}_3$  (Alfa Aesar 99.5%),  $\text{Yb}_2\text{O}_3$  (99.99%, acquired through Shanghai Zimei International Co., Ltd),  $\text{Nb}_2\text{O}_5$  (Aldrich 99.9%) and  $\text{Ga}_2\text{O}_3$  (Aldrich 99.99%) in a 36.33 : 0.21 : 27.21 : 36.25 weight% ratio. This off-stoichiometry formula is within the composition range with congruent melting that allows garnet crystal growth from the melt.<sup>28</sup> The mixture was heated in air to 1648–1673 K for several hours with intermediate regrinding. The garnet phase purity of the synthesized crystal precursor material was checked at RT using powder X-ray diffraction using a Bruker AXS D-8 Advance diffractometer with  $\text{Cu K}\alpha$  radiation. From this polycrystalline powder the single crystal was grown in air by the Czochralski technique. For this purpose we used a Cyberstar crystal growth equipment incorporating a radiofrequency (RF) coil fed by a Huttinger TruHeat MF 3020 power supply operated at 9.2 kHz. The crucible (40 mm in diameter and height) was made of platinum, and a

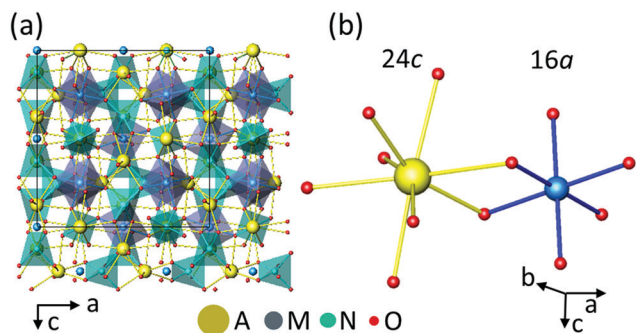


Fig. 1 (a) General view of the  $\text{A}_3\text{M}_2\text{N}_3\text{O}_{12}$  garnet structure. (b) Oxygen coordinations of the  $\text{AO}_8$  24c dodecahedra and  $\text{MO}_6$  16a octahedra.



platinum wire was used as the seed, which was rotated and pulled simultaneously. Samples for optical purposes were obtained by crystal cutting and polishing using conventional methods.

## 2.2 Structural and compositional analyses

Due to the low Yb<sup>3+</sup> doping (nominally 0.3 at% with regard to the dodecahedral site occupancy) of the currently studied 0.3 at%Yb:CNGG crystal, its structure should be very similar to that described for the undoped CNGG single crystal in one of our previous studies.<sup>14</sup> So, we shall adopt the crystal formula previously determined by the refinement of single crystal X-ray diffraction (XRD) data, *i.e.* {Ca<sub>0.985</sub>□<sub>D</sub>]<sub>3</sub>[Nb<sub>0.625</sub>Ga<sub>0.372</sub>□<sub>O</sub>]<sub>2</sub><sup>-</sup>(Ga<sub>0.821</sub>Nb<sub>0.102</sub>□<sub>T</sub>)<sub>3</sub>O<sub>12</sub>, □ stating for vacancies at 24c dodecahedral (curly brackets), 16a octahedral (square brackets) and 24d tetrahedral (parentheses) sites.

The low concentration of Yb in the studied garnet prevents their compositional determination using XRD or X-ray fluorescence methods. However, these methods were successfully used for heavily (> 10 at%) Yb-doped crystals. Thus, the actual Yb content of the used 0.3 at%Yb:CNGG crystal was determined by comparison of the integrated RT OA in this and in heavily Yb-doped crystals. This methodology provides a 0.08 at%Yb content for the grown crystal with regards to the dodecahedral occupancy.

## 2.3 Spectroscopic techniques

OA in the visible and NIR region was determined by using a Varian spectrophotometer, model Cary 5E, with a limiting spectral resolution of 0.04 nm at  $\lambda \approx 1000$  nm. An extensive 6 K OA study in the whole visible region using a thick ( $\approx 5.1$  mm) 0.3 at%Yb:CNGG sample discarded the contamination with any Ln different to the studied Yb<sup>3+</sup>. PL was excited either in a continuous wave (cw) with a tunable Ti-sapphire laser or pulsed (10 Hz) with a tunable Quanta-Ray MOPO-HF system providing ns laser pulses. PL light was dispersed in a SPEX ( $f = 34$  cm) spectrometer and detected using a 77 K cooled Ge photodiode in cw experiments, or with a Hamamatsu InP/InGaAs phototube (model H10330A-75) in lifetime measurements and time-resolved spectroscopy. In cw PL experiments the laser beam was chopped at  $\approx 200$  Hz and the PL signal recovered with a lock-in amplifier. Yb<sup>3+</sup> lifetime measurements were carried out using a thin crystal plate (60  $\mu$ m) in order to minimize emission reabsorption. Time-resolved spectroscopy was discriminated by a Stanford Research SR400 photon counter. For 6 K optical spectroscopic measurements a He close-cycle cryostat connected to a suitable temperature controller was used.

## 3. Results

The OA and PL spectra of Yb<sup>3+</sup> in the CNGG host originate from electronic transitions between ground <sup>2</sup>F<sub>7/2</sub> and excited <sup>2</sup>F<sub>5/2</sub> Yb<sup>3+</sup> multiplets. Both, the D<sub>2</sub> and C<sub>3i</sub> local symmetries of the dodecahedral 24c and octahedral 16a garnet sites, respectively, split these multiplets into four <sup>2</sup>F<sub>7/2</sub> ( $n = 0, 1, 2, 3$ ) and three <sup>2</sup>F<sub>5/2</sub> ( $n' = 0', 1', 2'$ ) Kramers doublets.

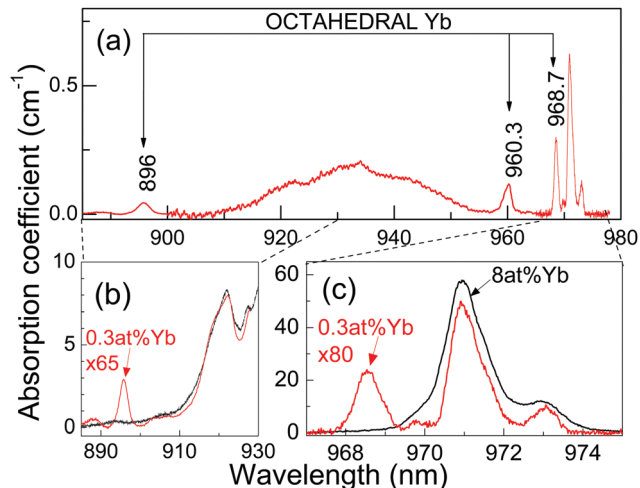


Fig. 2 (a) 6 K optical absorption spectrum of the 0.3 at%Yb:CNGG crystal (red line), and its comparison with that of the 8 at%Yb:CNGG crystal (black line) for (b) <sup>2</sup>F<sub>7/2</sub>(0) → <sup>2</sup>F<sub>5/2</sub>(2') and (c) <sup>2</sup>F<sub>7/2</sub>(0) → <sup>2</sup>F<sub>5/2</sub>(0') Yb<sup>3+</sup> transitions.

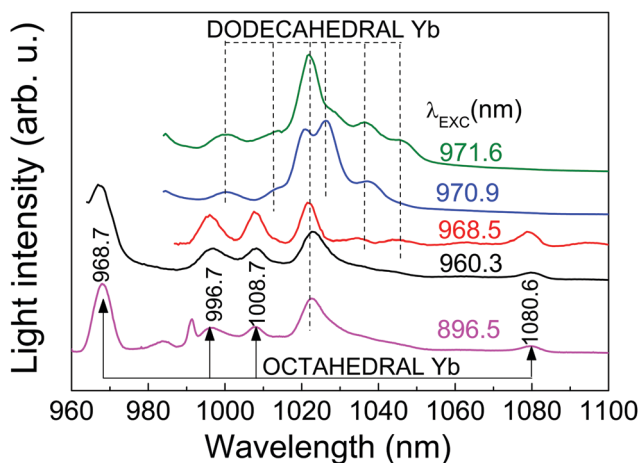


Fig. 3 Comparison of the 6 K photoluminescence spectra assigned to the octahedral 16a ( $\lambda_{\text{exc}} = 896.5, 960.3$  or  $968.5$  nm) and dodecahedral 24c ( $\lambda_{\text{exc}} = 970.9$  and  $971.6$  nm) Yb<sup>3+</sup> in the 0.3 at%Yb:CNGG single crystal.

The Yb<sup>3+</sup> spectra of heavily doped (> 1 at%Yb) CNGG crystals have been previously studied in detail.<sup>14,24–27</sup> So far, the crystallographic and spectroscopic studies only provided evidence for Yb incorporation in the dodecahedral 24c site. The 6 K OA and PL spectra consist in inhomogeneously and thermally broadened bands which hamper the accurate determination of some Yb<sup>3+</sup> energy levels. Fig. 2 and 3 show selected examples of the optical contributions of dodecahedral Yb in CNGG, while a more extensive dodecahedral Yb spectroscopic review is provided in the ESI.†

The only well resolved band in the 6 K spectra of 8 at%Yb:CNGG crystals is <sup>2</sup>F<sub>7/2</sub>(0) ↔ <sup>2</sup>F<sub>5/2</sub>(0') (shortly, 0 ↔ 0') at  $\lambda = 970.9$  nm (see Fig. 2c). Even this band is largely broadened by the different crystalline environments coexisting around the dodecahedral 24c site of Yb<sup>3+</sup>, since the spectral position of this 0 ↔ 0' transition is mainly related to the electric charge of cations/vacancies occupying the two edge-sharing tetrahedra



at the shortest distance ( $\sim 3.12 \text{ \AA}$ ) from the central  $24c \text{ Yb}^{3+}$ .<sup>24</sup> In fact, the small OA band at  $\lambda = 973 \text{ nm}$  corresponds to a dodecahedral  $\text{Yb}^{3+}$  center linked to a vacant edge-sharing tetrahedron.<sup>24</sup>

The 6 K OA (Fig. 2) and PL (Fig. 3) spectra of the 0.3 at%Yb:CNGG crystal show bands not observable in the corresponding spectra for heavily doped  $>1 \text{ at\%Yb:CNGG}$  crystals. The new well-resolved OA bands peak at  $968.7 \text{ nm}$  ( $10323 \text{ cm}^{-1}$ ),  $960.3 \text{ nm}$  ( $10413 \text{ cm}^{-1}$ ) and  $896 \text{ nm}$  ( $11161 \text{ cm}^{-1}$ ), while characteristic PL emissions at  $968.7 \text{ nm}$ ,  $996.7 \text{ nm}$ ,  $1008.7 \text{ nm}$  and  $1080.6 \text{ nm}$  are observed when exciting any of the three above listed OA bands (see Fig. 3). The absorption intensity of this new band set reaches 40% when the  $968.7 \text{ nm}$  new OA is compared with that of the dodecahedral  $\text{Yb} 0 \leftrightarrow 0'$  transition at  $\lambda = 970.9 \text{ nm}$ , see Fig. 2c. These new OA and PL band sets indicate the actual presence of a second type of Yb center coexisting in the garnet structure with the main dodecahedral  $\text{Yb}^{3+}$  center but with a much lower solubility limit, and thus, although present with low density, its contribution is not observable in the spectrum of the heavily doped Yb:CNGG crystals. In the following we show that this new center is compatible with the assumption of  $\text{Yb}^{3+}$  located at the octahedral 16a garnet site, and hereafter we shall refer to it as octahedral Yb.

Therefore, from the OA and PL bands experimentally determined for the octahedral  $\text{Yb}^{3+}$  center in CNGG, the complete set of  $\text{Yb}^{3+}$  energy levels can be established as  $0, 290, 410$  and  $1069 \text{ cm}^{-1}$  for the ground  ${}^2\text{F}_{7/2} (0, 1, 2, 3)$ , and  $10323, 10413$  and  $11161 \text{ cm}^{-1}$  for the excited  ${}^2\text{F}_{5/2} (0', 1', 2')$  multiplets.

In a further attempt to correlate these energy levels with the octahedral  $C_{3i} (\equiv S_6)$  symmetry of the 16a garnet site, a parametrization of CF effects in this site has been carried out. Since the large number of CF parameters accounting for the  $C_{3i}$  symmetry makes it unrealistic for any CF modeling to reproduce the sequence of  $\text{Yb}^{3+}$  energy levels, the often followed “descent of symmetry” procedure has considered the tetragonal bipyramidal  $D_{4h}$  symmetry as the better approach, *i.e.* the higher symmetry polyhedron with coordination number  $\text{CN} = 6$  that can be regarded as a distortion of an octahedron  $O_h$  whose fourfold rotation axis is chosen as the main axis. For the  $D_{4h}$  symmetry the CF potential is described by  $B_0^2, B_0^4, B_4^4, B_0^6$  and  $B_4^6$  CF parameters, preliminary  $O_h, B_0^4$  and  $B_0^6$  being the only independent parameters whose values were initially obtained by using the semi-empirical Simple Overlap Model.<sup>29</sup> Details of the procedure for the CF parametrization of  $16a \text{ Yb}^{3+}$  energy levels in CNGG are given in the ESI.† The energy levels of  $16a \text{ Yb}^{3+}$  in CNGG were adequately reproduced by using the set of free ion and  $D_{4h}$  CF parameters included in Table 1.

The  ${}^2\text{F}_{5/2} \text{ Yb}^{3+}$  PL intensity decay kinetics has been also studied as a further signature of the different symmetry of the two (octahedral and dodecahedral)  $\text{Yb}^{3+}$  centers observed in the 0.3 at%Yb:CNGG crystal. The  ${}^2\text{F}_{5/2} \text{ Yb}^{3+}$  PL time constant ( $\tau$ ) after  $970\text{--}973 \text{ nm}$  excitation through the  ${}^2\text{F}_{7/2}(0) \rightarrow {}^2\text{F}_{5/2}(0')$   $\text{Yb}^{3+}$  transition in the dodecahedral centers was shown to vary in the  $\tau = 800\text{--}450 \mu\text{s}$  range depending on the selected excitation/emission wavelength, *i.e.* the inhomogeneously modified dodecahedral center selected.<sup>24</sup> The increase of the Yb concentration

**Table 1** Free ion ( $E^0$  and  $\zeta$ ) and  $D_{4h}$  ( $B_0^2, B_0^4, B_4^4, B_0^6$  and  $B_4^6$ ) crystal field parameters (in  $\text{cm}^{-1}$ ) used to reproduce the sequence of  ${}^2\text{F}_{7/2}$  and  ${}^2\text{F}_{5/2}$  energy levels of  $16a \text{ Yb}^{3+}$  in the CNGG crystal

Parameter	$\text{Yb}^{3+}$ energy levels		
	Label	Observed ( $\text{cm}^{-1}$ )	Calculated ( $\text{cm}^{-1}$ )
$E^0$	4809.4	${}^2\text{F}_{7/2}(0)$	0
$\zeta$	2905.3	${}^2\text{F}_{7/2}(1)$	290
$B_0^2$	-64	${}^2\text{F}_{7/2}(2)$	410
$B_0^4$	2375	${}^2\text{F}_{7/2}(3)$	1069
$B_4^4$	1844	${}^2\text{F}_{5/2}(0')$	10323
$B_0^6$	-210	${}^2\text{F}_{5/2}(1')$	10413
$B_4^6$	251	${}^2\text{F}_{5/2}(2')$	11161

further reduces this time constant. An example of the PL kinetics is shown in Fig. 4a.

The octahedral Yb center of the 0.3 at%Yb:CNGG crystal exhibits completely different PL intensity decay kinetics, see Fig. 4b. Its time extent widely covers the 10 ms range, it is more sensitive to the sample heating from 6 K to RT than in the dodecahedral case and most often a non-single exponential behavior is observed. The PL decay kinetics excited at  $\lambda_{\text{EXC}} = 960.3 \text{ nm}$  are basically independent of the monitored wavelength

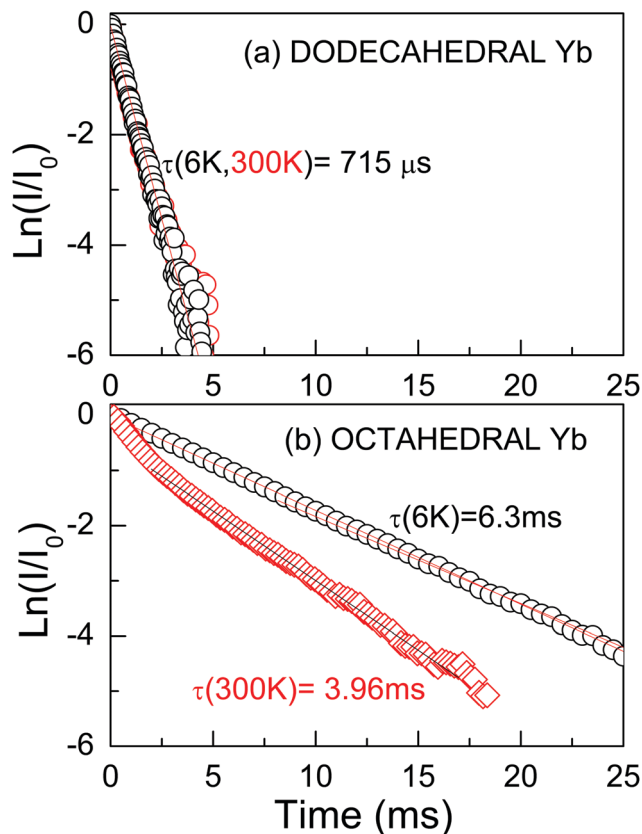


**Fig. 4** Comparison of the  ${}^2\text{F}_{5/2}$  photoluminescence intensity decay of the (a) dodecahedral  $24c \text{ Yb}^{3+}$  center,  $\lambda_{\text{EXC}} = 970.9 \text{ nm}$  and  $\lambda_{\text{EMI}} = 1022 \text{ nm}$ , and (b) octahedral  $16a \text{ Yb}^{3+}$  center,  $\lambda_{\text{EXC}} = 960.3 \text{ nm}$  and  $\lambda_{\text{EMI}} = 1080.6 \text{ nm}$ , of the 0.3 at%Yb:CNGG crystal. The points are the experimental results measured at 6 K (black points) and 300 K (red points). The lines are the fits of the long component of the corresponding decay.





( $\lambda_{\text{EMI}} = 968.7 \text{ nm}, 996.7 \text{ nm}, 1008.7 \text{ nm}$  or  $1080.6 \text{ nm}$ ), see the ESI† (Fig. S4). They most typical show a fast decay for  $t < 2 \text{ ms}$  and later a rather slow decay for the rest of the monitored time. This is understood as the overlapped contributions of the dodecahedral (short-lived) and octahedral (long-lived)  $\text{Yb}^{3+}$  centers. The long time tail of the decay can be fit to a single exponential law with a time constant  $\tau \approx 6\text{--}7 \text{ ms}$  at  $6 \text{ K}$  and  $\tau \approx 4 \text{ ms}$  at  $300 \text{ K}$ , *i.e.* the PL lifetime of the octahedral  $\text{Yb}^{3+}$  center is nearly one order of magnitude larger than that of the dodecahedral  $\text{Yb}$  one in the same crystal. This strong difference is consistent with the expected ED or MD  $\text{Yb}^{3+}$  PL contributions of these centers. For the non-centrosymmetric  $24c D_2$  dodecahedral site the contribution of ED transitions is expected to dominate the PL emission; thus the obtained  ${}^2F_{5/2} \text{Yb}^{3+}$  lifetime is in the range observed for crystals hosting  $\text{Yb}^{3+}$  in similar non-centrosymmetric sites, like YAG,  $\tau \approx 950 \mu\text{s}$ ,<sup>30</sup>  $\text{NaLn}(\text{WO}_4)_2$   $\tau \approx 300\text{--}500 \mu\text{s}$ ,<sup>31</sup> or  $\text{LnVO}_4$   $\tau \approx 250\text{--}350 \mu\text{s}$ .<sup>32</sup> However, as stated in the Introduction, the presence of a center of symmetry forbids ED transitions, thus MD ones are observed with similar or even larger intensities than for the ED contributions. Such MD transitions are characterized by long PL lifetimes, thus the much larger lifetime obtained for the so-called  $\text{Yb}$  octahedral center may be regarded as the ultimate probe of the occupancy by  $\text{Yb}^{3+}$  in the centrosymmetric  $16a$  crystal site of the CNGG host.

Once the origin of the described OA and PL features of the  $0.3 \text{ at\%Yb:CNGG}$  crystal has been clarified thanks to  $6 \text{ K}$  spectroscopy, its application as a probe of plasmonic induced radiation fields requires operation at RT. Fig. 5 shows a comparison of the OA spectra corresponding to  $0.3 \text{ at\%}$  and  $11.6 \text{ at\%Yb:CNGG}$  crystals, the spectroscopy of the latter being purely dominated by the dodecahedral  $\text{Yb}^{3+}$  contributions. It is obvious that excitation of the octahedral  $\text{Yb}^{3+}$  center at RT through its  $0 \rightarrow 0'$  transition at  $\lambda = 968.7 \text{ nm}$  is not possible because with increasing temperature the relative intensity of this band decreases and overlaps with the  $0 \rightarrow 0'$  (at  $\lambda = 972.3 \text{ nm}$ ) band tail corresponding to the dodecahedral  $\text{Yb}^{3+}$  center. However, the

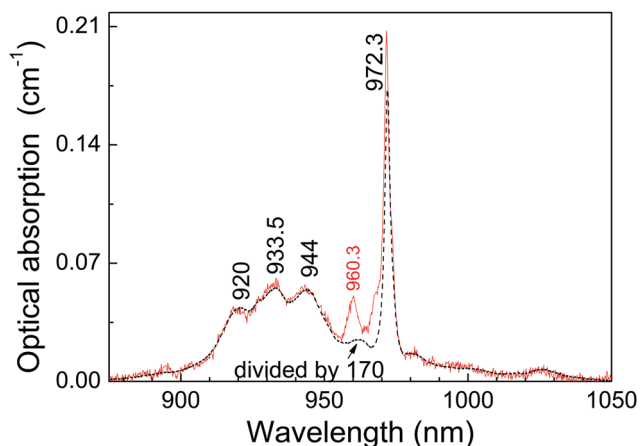


Fig. 5 Comparison of the  $300 \text{ K}$  OA spectra of  $0.3 \text{ at\%Yb:CNGG}$  (red continuous line) and  $11.6 \text{ at\%Yb:CNGG}$  (black dashed line) crystals. The spectral intensity of the latter crystal is divided by a factor of 170 to equal the intensity of the dodecahedral  $\text{Yb}^{3+}$  bands ( $920\text{--}944 \text{ nm}$ ) in both crystals.

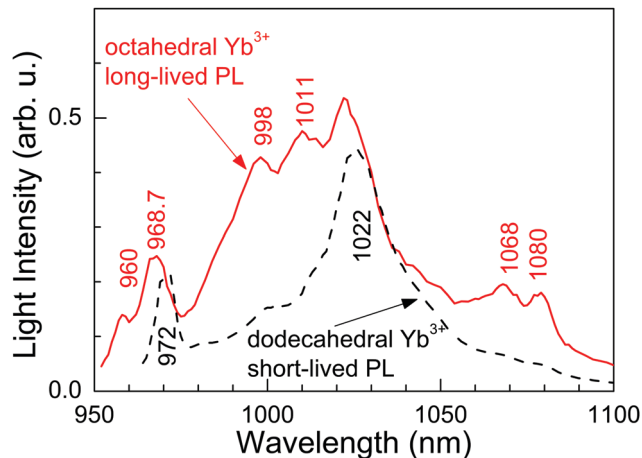


Fig. 6  $300 \text{ K}$  time-resolved photoluminescence emission of the  $0.3 \text{ at\%Yb:CNGG}$  crystal after excitation at  $\lambda = 960.3 \text{ nm}$  for different delay and gate times. Gate width of  $250 \mu\text{s}$  delay  $5 \mu\text{s}$  after laser pulse excitation (representative of the dodecahedral  $\text{Yb}^{3+}$  contribution, black dashed line) and gate width of  $8 \text{ ms}$  delay  $2.5 \text{ ms}$  (representative of the octahedral  $\text{Yb}^{3+}$  center, red continuous line).

comparison of the spectra at both  $\text{Yb}$  doping concentrations shows that the octahedral  $\text{Yb}^{3+} 0 \rightarrow 1'$  transition at  $\lambda = 960.3 \text{ nm}$  is clearly resolved from the background dodecahedral  $\text{Yb}$  contribution, the latter amounts to about 50% at this wavelength. Although the standard (integrated over time) cw PL spectra show little difference for excitation at the octahedral  $\text{Yb}^{3+}$  ( $\lambda = 960.3 \text{ nm}$ ) or in the side bands corresponding to the dodecahedral  $\text{Yb}^{3+}$  centers (see Fig. S3, ESI†), taking advantage of the different PL kinetics of both  $\text{Yb}^{3+}$  garnet centers, time-resolved spectroscopy can disclose the separate contributions of these two  $\text{Yb}^{3+}$  garnet centers.

Fig. 6 shows the RT time-resolved PL emission obtained for different delays and gate widths after the laser pulse ( $< 5 \text{ ns}$  of duration, tuned at  $\lambda = 960.3 \text{ nm}$ ) excitation. For short times ( $5 \mu\text{s}$  of delay and  $250 \mu\text{s}$  of gate width) the PL is dominated by the short-lived ED contributions of the dodecahedral  $\text{Yb}^{3+}$  center. Correspondingly, the emission spectrum shows a broad peak at  $1022 \text{ nm}$  characteristic of the PL observed in highly doped  $\text{Yb:CNGG}$ ,<sup>24,26</sup> which is also shown in Fig. 3 ( $\lambda_{\text{EXC}} = 971.6 \text{ nm}$ ). However, over a long time ( $2.5 \text{ ms}$  of delay and  $8 \text{ ms}$  of gate width) the spectrum is quite different, and matches the emission of the octahedral  $\text{Yb}^{3+}$  shown in Fig. 3. Although the contribution of the  $\lambda = 1022 \text{ nm}$  band is still present, this PL spectrum contains four well resolved emissions at  $\lambda = 998, 1011, 1068$  and  $1080 \text{ nm}$ , with intensities 2.80, 2.56, 2.94 and 3.76 times those corresponding to the dodecahedral  $\text{Yb}^{3+}$  contributions at the same wavelengths, respectively. The origin of the  $1068 \text{ nm}$  RT emission is related to the thermal redistribution of the  ${}^2F_{5/2}$  electronic population, and corresponds to the  ${}^2F_{5/2}(1') \rightarrow {}^2F_{7/2}(3)$  transition of the octahedral  $\text{Yb}^{3+}$  center.

## 4. Discussion

From  $6 \text{ K}$  OA and the excitation/emission PL spectra shown in Fig. 2 and 3, it has been disclosed that along the predominant



dodecahedral  $\text{Yb}^{3+}$  optical center associated with  $24c D_2$  symmetry in YAG-like garnets, another minority  $\text{Yb}^{3+}$  center with very different spectroscopic characteristics coexists in the 0.3 at%Yb:CNGG crystal.

Several CF considerations support the above conclusion. On one side, the experimental energies determined for the  $m_j$  levels of the so called 16a octahedral  $\text{Yb}^{3+}$  center are well reproduced by using a CF parameter set describing a centrosymmetric center, see Table 1. On the other side, the absolute CF splittings of  $1069 \text{ cm}^{-1}$  and  $838 \text{ cm}^{-1}$  for ground  ${}^2\text{F}_{7/2}$  and excited  ${}^2\text{F}_{5/2}$   $\text{Yb}^{3+}$  multiplets and their corresponding barycenters, lying at  $442 \text{ cm}^{-1}$  and  $10632 \text{ cm}^{-1}$  energies, respectively, are consistent with those found in other 6-fold oxygen coordinated Yb ionic oxides: in Yb-doped sesquioxides the  ${}^2\text{F}_{7/2}$  splitting ranges from  $1193 \text{ cm}^{-1}$  in  $\text{Lu}_2\text{O}_3$ ,<sup>33</sup> to  $1076 \text{ cm}^{-1}$  in  $\text{Sc}_2\text{O}_3$ ,<sup>34</sup>  $\Delta E({}^2\text{F}_{7/2}) = 1023 \text{ cm}^{-1}$  is found for  $\text{Ca}_4\text{YO}(\text{BO}_3)_3$  (with 6O-Yb-2B coordination),<sup>35</sup>  $964 \text{ cm}^{-1}$  in  $\text{Y}_2\text{SiO}_5$ ,<sup>34</sup> and  $900 \text{ cm}^{-1}$  in  $\text{Ba}_3\text{Lu}(\text{BO}_3)_3$ .<sup>34</sup> Smaller  $\Delta E({}^2\text{F}_{7/2})$  values in 6-fold oxygen coordinated Yb compounds are also found, for instance  $788 \text{ cm}^{-1}$  in  $\text{LiNbO}_3$ ,<sup>36</sup> or even below  $600 \text{ cm}^{-1}$  in Yb metalorganic complexes,<sup>37</sup> indicating a reduction of the CF strength on  $\text{Yb}^{3+}$ . In the latter case, a reduction of the effective Yb charge due to covalent bonds of oxygen to the neighboring organic ligands may contribute to the observed CF reduction, while in ionic crystals such CF strength reductions are partially ascribed to larger  $\text{Yb}^{3+}$  bond distances.

Even when the same  $\text{Yb}^{3+}$  coordination occurs in a given material the site symmetry influences the  ${}^{25+1}\text{L}_J$  multiplet splitting. Sesquioxides sharing 6-fold oxygen coordinated  $\text{Yb}^{3+}$  with and without a center of symmetry are a case similar to the present 0.3 at%Yb:CNGG that can guide us for the spectroscopic assignments. While efforts have been made in the assignment of usually experimentally incomplete  $\text{Yb}^{3+}$  energy level sets both for  $C_2$  and  $C_{3i}$  Yb centers of cubic sesquioxides,<sup>38,39</sup> mainly through the application of the barycenter plot law,<sup>34</sup> only CF analyses of  $24c$  dodecahedral  $\text{Yb}^{3+}$  energy levels have been attempted for garnet hosts.<sup>40,41</sup> These previously known data for cubic sesquioxides indicate that CF splittings of  ${}^2\text{F}_{7/2}$  and  ${}^2\text{F}_{5/2}$  are always wider and their corresponding barycenters are located at higher energies for centrosymmetric  $C_{3i}$   $\text{Yb}^{3+}$  centers than for the  $C_2$  ones, see Table 2 in ref. 38 and the ESI† (Table S1). The above indicated splittings for the  $C_{3i}$  16a  $\text{Yb}^{3+}$  center in the 0.3 at%Yb:CNGG crystal are considerably larger than those of  $\text{Yb}^{3+}$  in the noncentrosymmetric  $D_2$   $24c$  site in other garnet hosts, for instance,  $766 \text{ cm}^{-1}$  and  $352 \text{ cm}^{-1}$  for  ${}^2\text{F}_{7/2}$  and  ${}^2\text{F}_{5/2}$ , respectively, in YbAG, or  $624 \text{ cm}^{-1}$  and  $434 \text{ cm}^{-1}$  for YbGG, see Table S2 (ESI†). It could be assumed that larger CF splitting amplitudes for the centrosymmetric  $C_{3i}$  16a  $\text{Yb}^{3+}$  center are associated with the cooperative effect of considerably smaller bond distances for 16a  $\text{Yb}^{3+}$  than for  $\text{Yb}^{3+}$  in the dodecahedral environment as well as with an increase of the symmetry in the 16a center with regard to the  $24c$  one.

The solubility limit for  $\text{Yb}^{3+}$  incorporation at 16a positions in the CNGG crystal is rather low, obviously below 0.3 at% of the dodecahedral site. From the facts that the background optical absorption at  $\lambda = 960.3 \text{ nm}$  of dodecahedral  $\text{Yb}^{3+}$  centers in the 0.3 at%Yb:CNGG crystal is about 50% of the total, see Fig. 5,

and that the total Yb content was estimated from OA comparison as 0.08 at% of the dodecahedral site, the Yb density in the octahedral 16a garnet site can be roughly estimated to be  $\approx 5 \times 10^{18} \text{ cm}^{-3}$ . Such a low limit is in fact expected due to the large  $\text{Yb}^{3+}$  ionic radii ( $0.868 \text{ \AA}$  for VI coordination) compared to those of  $\text{Nb}^{5+}$  and  $\text{Ga}^{3+}$  ( $0.64 \text{ \AA}$  and  $0.62 \text{ \AA}$ , respectively, also for VI coordination). Due to the low solubility limit for Yb incorporation in the octahedral garnet site, direct evidence of corresponding MD transitions in the OA spectrum will diminish with the increase of Yb content in the crystal, and in fact the same OA bands from 16a  $\text{Yb}^{3+}$  can be also perceived with very low intensity in the 77 K OA spectrum of the 2 at%Yb:CNGG crystal reported by Voronko *et al.*,<sup>25</sup> while they are no longer observed in the OA spectrum of the 8 at%Yb:CNGG crystal, see Fig. 2b, since for these latter crystals ED transitions of  $\text{Yb}^{3+}$  in the dodecahedral garnet site have intensities several orders of magnitude stronger than those of the MD of  $\text{Yb}^{3+}$  in the octahedral garnet site.

Given that forced ED intraconfigurational f-f  $\text{Ln}^{3+}$  transitions from the centrosymmetric sites are strictly forbidden, the  ${}^2\text{F}_{5/2} \rightarrow {}^2\text{F}_{7/2}$  emission from 16a  $\text{Yb}^{3+}$  has a predominant MD character. Consequently, Yb:CNGG is able to provide simultaneously well-differentiated sets of  $\text{Yb}^{3+} {}^2\text{F}_{7/2} \leftrightarrow {}^2\text{F}_{5/2}$  ED and MD transitions, arising from  $24c$  and 16a garnet sites, respectively.

The evaluation of the MD contribution of the 16a  $\text{Yb}^{3+} {}^2\text{F}_{5/2}(0') \rightarrow {}^2\text{F}_{7/2}(1, 2, 3)$  ( $\lambda_{\text{EMI}} = 996.7, 1008.7$  and  $1080.6 \text{ nm}$ ) transitions can be performed by comparing the total decay rate derived from the measured lifetime value,  $\Gamma_{\text{total}} = 1/\tau$ , with the MD spontaneous emission rate,  $A_{\text{MD}} = A'_{\text{MD}} \times n_r^3$ , where the vacuum value  $A'_{\text{MD}}$  is predicted in ref. 12 and  $n_r = 1.96$  is the measured refractive index for CNGG at  $\lambda \approx 1000 \text{ nm}$ .<sup>14</sup> The MD branching ratio, defined as  $\beta_{\text{MD}} = A_{\text{MD}}/\Gamma_{\text{total}}$ , results in  $\beta_{\text{MD}} \approx 50\%$  for 16a  $\text{Yb}^{3+}$  in CNGG if the room temperature center lifetime is taken as  $\tau \approx 4 \text{ ms}$ , see Fig. 4b. This value is similar to previous  $\beta_{\text{MD}}$  values indicated for the  ${}^2\text{F}_{5/2}(0') \rightarrow {}^2\text{F}_{7/2}(0)$   $\text{Yb}^{3+}$  emission in crystals hosting  $\text{Yb}^{3+}$  in lattice sites with a center of symmetry, such as  $\text{SrF}_2$ ,  $\text{Rb}_2\text{NaYF}_6$  or  $\text{ScBO}_3$ .<sup>12</sup> Such crystals are difficult to grow and are not easily available with specific Yb doping, while unfortunately the MD branching ratio of  $\text{Yb}^{3+}$  in standard YAG is only 10.8%.<sup>12</sup> Therefore, even though the 16a  $\text{Yb}^{3+}$  center is present in the CNGG garnet with a low density, the strong MD character of its transitions makes them observable, which highlights the interest of the 0.3 at%Yb:CNGG crystal to be used for probing local magnetic fields in plasmonic resonances and metamaterials.

## 5. Conclusions

A new centrosymmetric octahedral  $\text{Yb}^{3+}$  center has been identified in the disordered  $\text{CaNbGa}$  garnet crystal with spectroscopic properties clearly different, both at 6 K and 300 K, from the usual dodecahedral  $\text{Yb}^{3+}$  center found in this and similar garnets. This new center, which shows favorable properties to be used as a probe for the intensity of magnetic fields radiated by plasmonic structures, operates around  $\lambda = 1 \mu\text{m}$  which is a



good compromise for lithographic fabrication and optical detection techniques. It is characterized by  ${}^2F_{7/2}(0-3) = 0, 290, 410, 1069 \text{ cm}^{-1}$  and  ${}^2F_{5/2}(0'-2') = 10323, 10413, 11161 \text{ cm}^{-1}$   $\text{Yb}^{3+}$   $m_j$  energy levels, which are consistent with the large CF splittings and barycenter energies expected for centrosymmetric  $\text{Yb}^{3+}$  centers in ionic compounds, their individual positions being well reproduced by a CF simulation assuming a lower, but still with inversion center,  $D_{4h}$  symmetry.

The probe center can be operated at room temperature by excitation at  $\lambda = 960.3 \text{ nm}$  and with best sensitivity detection near  $\lambda = 1080 \text{ nm}$ , although other additional detection channels are found at  $\lambda = 998, 1011$  and  $1068 \text{ nm}$ . The coexistence of dodecahedral and octahedral  $\text{Yb}^{3+}$  centers in the same crystal with roughly similar densities allows the detection of reference ED and signal MD PL contributions corresponding to the above centers, respectively. Separation of both contributions has been conveniently made by using time-resolved spectroscopy, since ED  $\text{Yb}^{3+}$  PL is short-lived ( $\tau < 0.8 \text{ ms}$ ) and the MD one is long-lived ( $\tau \approx 4 \text{ ms}$ ). The measured MD branching ratio in the studied garnet,  $\beta \approx 50\%$ , is equivalent to those previously reported in other centrosymmetric hosts, but the easy growth in air of the present  $\text{CaNbGa}$  garnet with congruent melting at  $\approx 1470 \text{ }^\circ\text{C}$  will facilitate the fabrication of the required plasmonic or metamaterial structures in comparison for instance with  $\text{Y}_2\text{O}_3$  whose crystal availability is very limited due to its high melting point of  $\approx 2490 \text{ }^\circ\text{C}$ .

## Conflicts of interest

There are no conflicts to declare.

## Acknowledgements

This work has been supported by the Spanish Ministry of Economy and Competitiveness and by the European Regional Development Fund through project RTI2018-094859-B-I00. CSIC support for Open Access publication and advice of Prof. Rafael Valiente on time-resolved spectroscopic measurements are acknowledged.

## References

- W. T. Carnall, P. R. Fields and K. Rajnak, *J. Chem. Phys.*, 1968, **49**, 4424.
- Q. Thommen and P. Mandel, *Opt. Lett.*, 2006, **31**, 1803.
- N. Noginova, G. Zhu, M. Mavy and M. A. Noginov, *J. Appl. Phys.*, 2008, **103**, 07E901.
- N. Noginova, Y. Barnakov, H. Li and M. A. Noginov, *Opt. Express*, 2009, **17**, 10767.
- N. Yang, Y. Tang and A. E. Cohen, *Nano Today*, 2009, **4**, 269.
- X. Ni, G. V. Naik, A. V. Kildishev, Y. Barnakov, A. Boltasseva and V. M. Shalaev, *Appl. Phys. B: Photophys. Laser Chem.*, 2011, **103**, 553.
- T. H. Taminiau, S. Karaveli, N. F. van Hulst and R. Zia, *Nat. Commun.*, 2012, **3**, 979.
- S. Karaveli and R. Zia, *Opt. Lett.*, 2010, **35**, 3318.
- S. Karaveli and R. Zia, *Phys. Rev. Lett.*, 2011, **106**, 193004.
- M. Kasprczyk, S. Person, D. Ananias, L. D. Carlos and L. Novotny, *Phys. Rev. Lett.*, 2015, **114**, 163903.
- C. M. Dodson, J. A. Kurvits, D. Li, M. Jiang and R. Zia, *Opt. Mater. Express*, 2014, **4**, 2441.
- C. M. Dodson and R. Zia, *Phys. Rev. B: Condens. Matter Mater. Phys.*, 2012, **86**, 125102.
- L. DeLoach, S. Payne, L. Chase, L. Smith and W. Kway, *IEEE J. Quantum Electron.*, 1993, **29**, 1179.
- E. Castellano-Hernández, M. D. Serrano, R. J. Jiménez-Riobóo, C. Cascales, C. Zaldo, A. Jezowski and P. A. Loiko, *Cryst. Growth Des.*, 2016, **16**, 1480.
- S. Geller, *Z. Kristallogr.*, 1967, **125**, S1 (and refs. therein).
- L. Suchow, M. Kokta and V. J. Flynn, *J. Solid State Chem.*, 1970, **2**, 137.
- L. Suchow and R. Mondegarian, *J. Solid State Chem.*, 1973, **6**, 553.
- B. V. Mill', *Sov. Phys. Crystallogr.*, 1975, **19**, 653.
- M. Asano and J. A. Koningstein, *Chem. Phys.*, 1979, **42**, 369.
- D. Lévy and J. Barbier, *Acta Crystallogr., Sect. C: Cryst. Struct. Commun.*, 1999, **55**, 1611.
- M. O. Ramírez, L. E. Bausá, E. Cavalli and E. Bovero, *J. Appl. Phys.*, 2006, **99**, 013507.
- H. G. Liu, W. C. Zheng and W. L. Feng, *Philos. Mag.*, 2008, **88**, 3075.
- A. Kaminska, M. G. Brik, G. Boulon, M. Karbowski and A. Suchocki, *J. Phys.: Condens. Matter*, 2010, **22**, 255501.
- M. D. Serrano, J. O. Álvarez, C. Zaldo, J. Sanz, I. Sobrados, J. A. Alonso, C. Cascales, M. T. Fernández-Díaz and A. Jezowski, *J. Mater. Chem. C*, 2017, **5**, 11481.
- Y. K. Voronko, A. V. Popov, A. A. Sobol and S. N. Ushakov, *Inorg. Mater.*, 2006, **42**, 1133.
- V. E. Shukshin, *Phys. Wave Phenom.*, 2009, **17**, 165.
- V. Lupei, A. Lupei, C. Gheorghe, L. Gheorghe, A. Achim and A. Ikesue, *J. Appl. Phys.*, 2012, **112**, 063110.
- K. Shimamura, M. Timoshechkin, T. Sasaki, K. Hoshikawa and T. Fukuda, *J. Cryst. Growth*, 1993, **128**, 1021.
- P. Porcher, M. C. dos Santos and O. Malta, *Phys. Chem. Chem. Phys.*, 1999, **1**, 397.
- D. S. Sumida and T. Y. Fan, *Opt. Lett.*, 1994, **19**, 1343.
- E. V. Zharikov, C. Zaldo and F. Díaz, *MRS Bull.*, 2009, **34**, 271 (and refs. therein).
- J. Liu, X. Mateos, H. Zhang, J. Wang, M. Jiang, U. Griebner and V. Petrov, *Opt. Lett.*, 2005, **30**, 3162.
- D. C. Brown, Z. Fleischman, L. D. Merkle, L. D. Sanjeewa, C. D. McMillen and J. W. Kolis, *Appl. Phys. B: Photophys. Laser Chem.*, 2020, **126**, 62.
- P. Haumesser, R. Gaumé, B. Viana, E. Antic-Fidancev and D. Vivien, *J. Phys.: Condens. Matter*, 2001, **13**, 5427.
- A. Lupei, G. Aka, E. Antic-Fidancev, B. Viana, D. Vivien and P. Aschehoug, *J. Phys.: Condens. Matter*, 2002, **14**, 1107.
- E. Montoya, J. A. Sanz-García, J. Capmany, L. E. Bausá, A. Dening, T. Kellner and G. Huber, *J. Appl. Phys.*, 2000, **87**, 4056.



- 37 J. Wang, J. J. Zakrzewski, M. Heczko, M. Zychowicz, K. Nakagawa, K. Nakabayashi, B. Sieklucka, S. Chorazy and S. Ohkoshi, *J. Am. Chem. Soc.*, 2020, **142**, 3970 (and ref. 78 and 79 therein).
- 38 Y. Guyot, M. Guzik, G. Alombert-Goget, J. Pejchal, A. Yoshikawa, A. Ito, T. Goto and G. Boulon, *J. Lumin.*, 2016, **170**, 513.
- 39 E. Antic-Fidancev, J. Holsa and M. Lastusaari, *J. Phys.: Condens. Matter*, 2003, **15**, 863.
- 40 L. Hong-Gang, Z. Wen-Chen and F. Wen-Lin, *J. Lumin.*, 2010, **130**, 103.
- 41 L. Hong-Gang, G. Paweł and R. Czesław, *J. Lumin.*, 2011, **131**, 2690.

